P2.41

COLLISION RATE ENHANCEMENT IN TURBULENT CLOUDS OF DIFFERENT TYPES

M. Pinsky and A. Khain*
The Hebrew University of Jerusalem, Israel

1. INTRODUCTION

It is widely accepted now that turbulence enhances the rate of particle collisions (see overviews by Pinsky et al 2000; Vaillancourt and Yau 2000; Shaw 2003). There exist three major mechanisms that turbulence affects the collision rate: a) increase in the relative particle velocity (or increase in the swept volume); this effect is also known as turbulent transport effect; b) formation of concentration inhomogeneity (particle clustering), and c) turbulence effect on the hydrodynamic drop interaction (HDI) that leads to an increase in the collision efficiency. Published reports dedicated to turbulence effects on HDI are quite scarce. Small amount of such studies is surprising because gravity-induced values of the collision efficiencies are small (0.001-0.1) (Pruppacher and Klett 1997) keeping a large volume for turbulence to increase the collision efficiency and the collision rate.

Almeida (1979) and Koziol and Leighton (1996) analyzed the effects of turbulent vortices of scales smaller than HDI, which normally fall well into the viscous range. The effect of these low - energy vortices on the collision efficiency was shown to be negligibly small (Pruppacher and Klett, 1997). Further estimations made by Pinsky et al (1999a) and Pinsky and Khain (2004), who took into account the effects of turbulent vortices within the inertial and transition ranges, indicated that turbulence can significantly (by hundred percent) increase collision efficiencies and kernels between cloud droplets. Direct numerical simulations (DNS) performed recently by Franklin et al (2004) and Wang et al (2005a) also indicate a pronounced increase in the collision efficiency in a turbulent flow generated by DNS models.

Note that DNS are conducted with the Taylor microscale Reynolds numbers Re_λ ranged from 70 to 200. These values are much smaller than those typical of atmospheric turbulence (about $(1 \div 5) \times 10^4$). Pinsky and Khain (2004) calculated the collision efficiencies and kernels in a turbulent flow with high Re_λ typical of atmospheric clouds. In that study, however, only the Lagrangian accelerations were taken into account, while the effects of turbulent shears were disregarded. Pinsky et al (2006a) analyzed the effects of both turbulent accelerations and shears on droplet collisions in the absence of HDI. To perform the calculations, a statistical representation of a turbulent flow was proposed based on the results of the scale

---

* *Corresponding author address: Prof. Alexander Khain, The Hebrew University of Jerusalem, Dept. Atmos. Sciences, Israel, khain@vms. huji.ac.il*

analysis of characteristics of turbulence and droplet motion. The statistical properties of turbulent flow were represented by a set of non-correlated samples of turbulent shears and the Lagrangian accelerations. Each sample can be assigned to a certain point of a turbulent flow. Each such point can be surrounded by a small "elementary" volume with linear length scales of the Kolmogorov length scale, within which the Lagrangian acceleration and turbulent shears were regarded as uniform in space and invariable in time. Using the statistical model (Pinsky et al 2004), long series of turbulent shears and accelerations were generated reproducing the probability distribution functions (PDFs) of these quantities at high Reynolds numbers as they had been obtained in recent laboratory and theoretical studies. The swept volumes of droplets were calculated for each sample of the acceleration-shear pair, and the PDF of swept volumes was calculated for the parameters typical of cloud turbulence. It was found that the magnitude of the mean swept volume increases both with the Reynolds number and the dissipation rate. At the same time such increase for cloud droplets did not exceed ~60 % even under turbulent conditions typical of strong cumulus clouds ($\mathrm{Re}_\lambda = 2 \cdot 10^4$, $\varepsilon = 0.1\ m^2 s^{-3}$).

Pinsky et al (2006b) extended the approaches developed in Pinsky et al (2006a) for the purpose of calculating turbulence effects on HDI for cloud droplets with radii below 20 μm. In this presentation we briefly describe the method of calculation of collision efficiency and collision kernels developed by Pinsky et al (2006b) and present tables of enhancement factors for collision kernels as compared to the gravitation collision kernels. Collision efficiencies and collision kernels between cloud droplets are calculated under turbulent conditions typical of actual clouds at 1000 mb and 500 mb pressure levels. Effects of turbulence on the droplet size distribution (DSD) is illustrated by solving the stochastic collision equation for different dissipation rates and Re_λ.

2. PHYSICAL MODEL

The essential parts and general concepts of the study are described by Pinsky et al (2006a). For the sake of convenience, we briefly repeat here the main points and definitions introduced therein, and concentrate on the calculation of collision efficiencies.

Droplet motion in a turbulent flow at small scales is determined by gravity, the turbulent Largangian accelerations A_i and the tensor of turbulent shears S_{ij} ($i, j = 1,2,3$). Statistical properties of a turbulent flow are represented here by a set of non-correlated samples of turbulent shears and Lagrangian accelerations. Each sample can be assigned to a certain point of the turbulent flow. Since the spatial and temporal scales of turbulent shears and acceleration exceed the corresponding Kolmogorov scales several fold, each such point can be surrounded by a small "elementary" volume with the characteristic lengths and time scales equal to the corresponding Kolmogorov scales, in which the Lagrangian acceleration and turbulent shears are considered to be uniform in space and invariable in time.

The quantities characterizing collisions were calculated for each elementary volume. As it was shown by Pinsky et al (2006a), droplet velocity relative to the environment flow relaxes in the majority of cases to its adapted (quasi-stationary) value $V_j^{'\,ad}$ within the time periods shorter than the temporary scales of turbulent shears and accelerations. It means that within each elementary volume we can use adapted relative droplet velocities when dealing with droplet collisions. The equation system for the motion of isolated droplets can be written in this case as:

$$V_j^{'\,ad}\left(\frac{1}{\tau}\delta_{ij}+S_{ij}\right)=A_i+V_tS_{3i} \qquad (1)$$

$$\frac{dx_i}{dt}=V_i \quad =S_{ij}x_j+V_t\delta_{3i}+V_i^{'\,ad} \quad , \qquad (2)$$

where $V_i^{'\,ad}=V_i-W_i-V_t\delta_{i3}$, and V_i, W_i and V_t are droplet velocity, air velocity and the terminal fall velocity induced by gravity, respectively; τ is the drop relaxation time that is the measure of droplet inertia. For cloud droplets $\tau=(2/9)(\rho_w/\rho_a)(a^2/\nu)$, where ρ_w *and* ρ_a are the water and air densities, respectively, and a is the droplet radius. Eq. (1) is valid if τ is less than a certain critical value depending on the shear tensor. Cases when this condition was not satisfied for droplets with radii below 20 μm were quite rare and rejected from the analysis. Taking into account that these cases are very rare, neglecting those does not affect the mean values of swept volumes and collision efficiencies. As regards the PDF of collision efficiencies, these rare cases contribute to the far tail only.

The equation for the relative droplet velocity between two non-interacting droplets $\widetilde{V}_i=V_{2i}-V_{1i}$ within an elementary turbulent volume can be written as (see Pinsky at al 2006a):

$$\widetilde{V}_i=\frac{d\widetilde{x}_i}{dt}=S_{ij}x_j+\widetilde{V}_i' \qquad (3)$$

where $\widetilde{x}_i=x_{2i}-x_{1i}$ is the position vector between the centers of two droplets, and $\widetilde{V}_i' \;=V_{2i}^{'ad}-V_{1i}^{'ad}+(V_{2t}-V_{1t})\delta_{i3}$. One can see from (3) that the relative velocity between non-interacting droplets does not depend on the location of the droplet pair within the elementary volume, but rather on the vector connecting their centers only.

The growth rate of a droplet with radius a_2, caused by collisions with droplets of radius a_1, is determined by the flux Φ of the a_1-radius droplets onto the a_2-radius droplet. This flux is assumed to cross the spherical surface of (a_1+a_2) radius, and hence can be expressed as:

$$\Phi=\frac{1}{a_1+a_2}\int_{\Omega_+}N_1\widetilde{V}_i\widetilde{x}_i d\Omega_+ \quad , \qquad (4)$$

where N_1 is the concentration of the a_1- radius droplets and Ω_+ is the fraction of the spherical surface, where $\widetilde{V}_i\widetilde{x}_i<0$. **Fig. 1** illustrates this definition of the drop flux. In the figure, the (a_1+a_2) radius sphere represents the target;

the curves with arrows represent relative droplet trajectories.

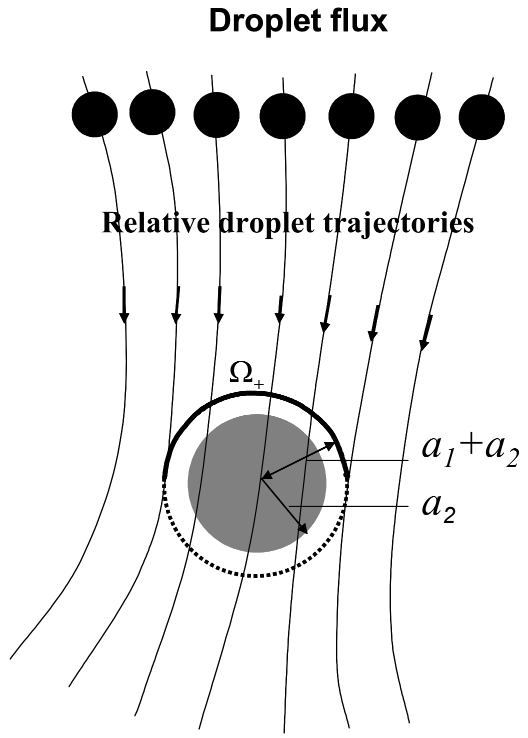

Figure 1. Illustration of the drop flux definition. The (a_1+a_2)- radius sphere represents the target; the curves with arrows represent relative droplet trajectories. Surface Ω_+ represents the area where relative trajectories are directed inside the target.

Taking into account that the inertia-induced fluctuations of droplet concentration for cloud droplets are quite small (especially if the differential sedimentation velocity is taken into account, see abstract 14.3), the concentration N_1 can be considered constant within elementary volumes. Consequently, instead of the droplet flux, it appears more convenient to deal with relative velocity fluxes which can be defined as $F=\frac{\Phi}{N}$. Using (3) and (4), one can express the swept volume normalized to its value in the pure gravity case as:

$$S_v = \frac{1}{\pi(a_1+a_2)^3|V_{t2}-V_{t1}|}\int_{\Omega_+}\left(S_{ij}\tilde{x}_j\tilde{x}_i+\tilde{V}_i'\tilde{x}_i\right)d\Omega_+ \qquad (5)$$

As it follows from eqs. (1) and (5), to calculate droplet flux in the absence of HDI one must know the Lagrangian acceleration and the turbulent shear in each elementary volume. Pinsky et al (2006a) calculated long series of acceleration-shear pairs (or samples of elementary volumes) using a statistical model by Pinsky at al (2004). This model reproduces the probability distribution functions (PDF) of accelerations and the shears at high Re_λ as they were obtained in the recent laboratory studies (Belin et al 1997, La Porta et al 2001) and theoretical studies (Hill 2002). The same series of accelerations and turbulent shears are used to calculate collision efficiencies.

3. DEFINITION AND CALCULATION OF COLLISION EFFICIENCY

3.1 Definition of the collision efficiency

The collision efficiency *E* between two populations of a_1 and a_2- radii droplets is generally defined as the ratio of the droplet fluxes:

$$E(a_1,a_2)=\Phi_{HDI}/\Phi_{noHDI} \quad , \qquad (6a)$$

where Φ_{HDI} is the flux of a_1 –radii droplets onto a_2-radius droplet when colliding droplets experience HDI, and Φ_{noHDI} is the droplet flux in the absence of HDI. As the droplet concentration is assumed to be uniform throughout the elementary volume, the collision efficiency can be also defined as the ratio of relative velocity fluxes:

$$E(a_1, a_2) = \frac{F_{HDI}}{F_{noHDI}} \qquad (6b)$$

Thus, evaluation of the collision efficiency requires calculation of these fluxes under turbulent conditions typical of atmospheric clouds.

The procedure of calculation of droplet fluxes is described below.

a. *The technique of calculation of a flux in the absence of HDI.* To calculate this velocity flux (see Pinsky et al 2006a for more detail), the $(a_1 + a_2)$- radius target surface is divided into hexagonal pixels of equal square dΩ_+ using the icosahedron-based method (Tegmark 1996). The number of pixels has been chosen so as to be large enough to provide a high accuracy of calculations. The high resolution is especially important when calculating small collision efficiencies, since the fluxes are determined with the accuracy equal to the magnitude of the flux crossing a single pixel. In the absence of HDI, the velocity flux dF_k corresponding to the k-th pixel is calculated as:

$$dF_k = \frac{\left(S_{ij}\tilde{x}_{0j}\tilde{x}_{0i} + \tilde{V}_i'\tilde{x}_{0i}\right)d\Omega_+}{a_1 + a_2} \qquad (7)$$

The flux F_{noHDI} was calculated by integrating (7) over the surface Ω_+.

b. *Calculation of the droplet flux in the presence of HDI.* To perform this task, the following procedure was used. We start the description with the simplest case, namely when droplet trajectories in the presence of HDI do not deviate significantly from the non-disturbed trajectories (see **Figure 2)**. Using Eq. (3) we calculated the non-disturbed relative trajectories of droplets, which cross the spherical surface $\left|\tilde{x}_{0i}\right| = a_1 + a_2$ (the dashed circle in Fig. 2) during droplet approach in the absence of HDI. For this purpose, Eq. (3) was integrated back in time using the initial positions located on the target surface as it was discussed above. Such trajectories were calculated beginning from the centre of each pixel. The backward trajectories were calculated for the same time periods, by the end of which the droplets were separated by the distance of about 10 radii of the larger droplet in the droplet pair. This distance is large enough to provide accurate calculation of mutual droplet tracks (Pruppacher and Klett, 1997).

The final points of the backward trajectories form the surface of the second order referred to in Fig. 2 as A_{noHDI}. As a result, there is a one-to-one pixel correspondence between the points of surface A_{noHDI} and the points on the target surface $\left|\tilde{x}_{0i}\right| = a_1 + a_2$. Trajectories connecting the corresponding pixels (e.g. A-A', B-B') can be regarded as a stream tube that transports the flux dF_k (7).

To determine the velocity flux in the presence of HDI, we calculated the absolute trajectories of droplets of radius a_1 and a_2 forward in time, as shown in **Figure 2**. These trajectories start at the final points of the backward trajectories, i.e., from the centers of the pixels located on the surface A_{noHDI}. Two examples of such trajectories that start from points A' and B' are schematically shown in Fig.2. Due to HDI, only a certain fraction of the trajectories leads to collisions (for example, the droplet starting at point A' collides, while the droplet that starts at point B' does not). Taking into account that each of these trajectories is responsible for its own velocity flux dF_k, we calculated the total velocity flux F_{HDI} in the presence of HDI by summing up the elementary fluxes of the trajectories which lead to droplet collisions. The ratio of the fluxes with and without HDI determines the value of the collision efficiency.

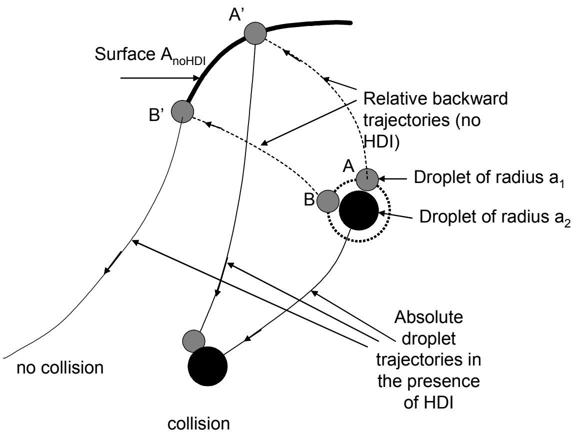

***Figure 2**. Scheme illustrating the procedure of calculation of droplet velocity fluxes in case HDI is taken into account. Notations: the* $(a_1 + a_2)$ *radius spherical surface is the target. (see text for more detail) The final points of the backward relative trajectories (e.g. AA', BB') form* A_{noHDI} *surface. The* A_{noHDI} *surface is divided into pixels, thus the k-th pixel on the surface corresponds to the velocity flux* dF_k. *The absolute trajectories of* a_1*-radius droplets start from the centers of all the pixels situated on the* A_{noHDI} *surface. In the presence of HDI, only a fraction of these trajectories leads to droplet collision.*

Figure 3 illustrates the definition of the collision efficiency. The black sphere in the figure represents the target of $(a_1 + a_2)$ radius. The surface A_{noHDI} represents the source of the total flux F_{noHDI}. The fraction of this surface denoted as A_{HDI} forms the flux F_{HDI} of droplets that collide with the target, when HDI is taken into account.

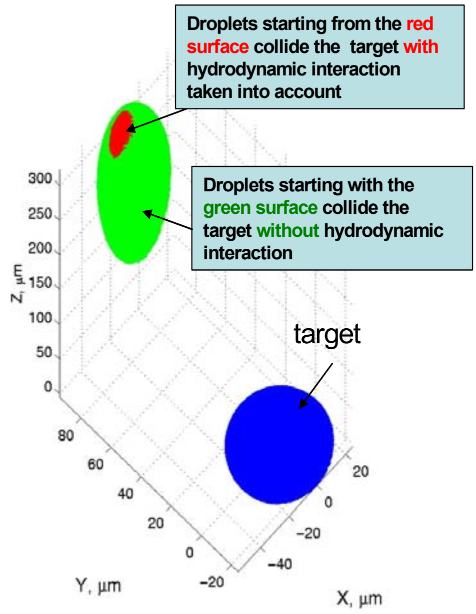

***Figure 3**. An example of the droplet collision geometry for 10* μm *and 20* μm *- radii droplet pair for one of the samples of the turbulent flow.*

Notations: the blue sphere is the (a_1+a_2) *radius target. The* A_{noHDI} *surface formed by the final points of the backward-in-time trajectories is shown in the upper part of the figure, marked green. Droplets that start moving from this surface collide with the target in the absence of hydrodynamic droplet interaction. Droplets starting from the area* A_{HDI} *, marked red, collide with the target in the presence of hydrodynamic droplet interaction. The figure illustrates the simplest case when the* A_{HDI} *area is fully located inside* A_{noHDI} *area.*

Fig. 3 illustrates the case when the surface A_{HDI} is fully located within the surface A_{noHDI}. In some cases, however, HDI affects the tracks of approaching droplets so significantly that the area A_{HDI} is not fully located within the surface A_{noHDI}. To take these cases into account, a more complicated algorithm was used related to utilization of an ancillary spherical surface of a larger radius that surrounds the (a_1+a_2)-radius target.

It is noteworthy that in the pure gravity case the definition (6) of collision efficiency as the ratio of velocity fluxes reduces to the commonly used definition of collision efficiency as the ratio of collision areas and areas of geometrical cross-sections (Pruppacher and Klett 1997). As it follows from eq.(3), in calm air the relative velocity between droplets at the infinity is equal to the difference between their terminal fall velocities. Thus, in expression (7) for droplet fluxes, this constant relative velocity can be factored out of the integral, and fluxes of relative velocity (or droplets) thus become proportional to the area of the cross-sections of the flux tubes (the areas of pixel projections on the horizontal plane). As a result, in the pure gravity case the ratio $\frac{F_{HDI}}{F_{noHDI}}$ is transformed into the ratio of the collision and geometrical cross-section areas.

3.2 The modification of the superposition method

In order to perform collision efficiency calculations, the problem of hydrodynamic interaction between two spheres moving in the airflow is considered. We use the superposition method (Pruppacher and Klett 1997), according to which each sphere is assumed to move in a flow field induced by its counterpart moving alone. The method was first proposed by Langmuir (1948), and was later successfully used by many investigators (Shafrir and Gal-Chen 1971; Lin and Lee 1975; Schlamp et al 1976) for the calculation of collision efficiencies between droplets within a wide range of sizes. The superposition method was used by Pinsky et al (2001) for calculation of detailed tables of gravity-induced collision efficiencies for droplets within the 1 μm to 300 μm-radii range. The calculated values of collision efficiencies allowed us to obtain an accurate reproduction of drop-collector growth measured in the vertical wind tunnel at the University of Mainz (Vohl et al 1999). Wang et al (2005b) have recently shown that the center-point formulation of the superposition method provides a good agreement with the exact solutions available. Pinsky et al (1999a, 2001, the present study) use the center-point formulation of the superposition method for calculation of collision efficiency in a turbulent flow.

According to the superposition method, the perturbed velocity field induced by each drop in calm air is calculated as for the case of a single isolated droplet. Each of the interacting drops experiences the velocity field induced by its counterpart droplet. The expression for the induced velocity field can be found in Pruppacher and Klett (1997) and in Pinsky et al (1999).

In the present study we apply a modified superposition method allowing simplification of the governing equations. The idea of the modification is the following: each droplet' velocity V_i' relative to the surrounding air is represented as the sum of two components: a non-disturbed velocity $\widehat{V}_i'$ without the impact of the counterpart droplet, and a disturbed velocity $\breve{V}_i'$, induced by the counterpart droplet. As it was shown by Pinsky et al (2006a), $\widehat{V}_i'$ rapidly adapts to $V_i^{'ad}$, which depends on the Largangian acceleration, turbulent shear and the terminal fall velocity of the droplet. Within each elementary volume, $V_i^{'ad}$ is constant with a high accuracy. This allows us to simplify the corresponding motion equation by utilizing the condition $\widehat{V}_i'$ = $V_i^{'ad}$ (see eqs. 1 and 8b). In the course of HDI the velocity component $\breve{V}_i'$ can experience significant changes caused by the rapidly varying velocity field induced by the counterpart droplet. Hence, the time derivative in the equation for the component $\breve{V}_i'$ should be taken into account (see eq. 8a).

As a result, the system of equations governing the motion of any interacting droplets can be reduced to the following form:

$$\frac{d\breve{V}_i'}{dt} = -\breve{V}_j'\left(\frac{1}{\tau}\delta_{ij}+S_{ij}\right)+\frac{1}{\tau}u_i^*(x_i) \tag{8a}$$

$$\widehat{V}_i'\left(\frac{1}{\tau}\delta_{ij}+S_{ij}\right)=A_i+V_tS_{3i} \tag{8b}$$

$$V_i=\frac{dx_i}{dt}=S_{ij}x_j+V_t\delta_{3i}+\widehat{V}_i'+\breve{V}_i' \tag{8c}$$

To describe the mutual motion and collision of two interacting droplets, two coupled equation systems similar to (8a-8c) should be solved. Since $\breve{V}_i'$ tends to zero at large separations (~10 radii of the larger droplet), the initial droplet velocity is equal to

$$V_i=S_{ij}x_j+V_i^{'ad}+V_t\delta_{3i} \tag{9}$$

In the absence of HDI, $\breve{V}_i'=0$ and eqs. (8) coincide with eqs. (12-13 in Pinsky et al 2006a) for the motion of non-interacting droplets. Note also that in calm air $(A_i=0;S_{ij}=0)$ eqs. (8) are reduced to the classical system of equations for the superposition method in the pure gravity case.

The advantage of the approach proposed is that equation (8a) for $\breve{V}_i'$ contains the “viscous” term (the first right-hand one), which allows the utilization of a simple and computationally efficient time-explicit middle point numerical scheme.

The following verification of the accuracy of calculations was performed:

- *Sensitivity of trajectory integration to value of time step.* The time step Δt of integration of eqs (8a-c) was chosen $\Delta t \leq 0.1\tau_s$, where τ_s is the characteristic relaxation time of the smallest droplet in the droplet pair. Calculations showed that further decrease of the time step did not influence the results.
- *Sensitivity to the number of pixels* used for calculation of droplet fluxes. The accuracy is determined by the resolution that can be evaluated as *4/n*, where *n* is the number of pixels covering the target surface. For spheres of $(a_1 + a_2)$ radius, n=2252 was used, so that the error in the calculations of droplet velocity fluxes did not exceed 0.2 %. As was mentioned above, the number of pixels was increased proportionally to the surface square of the ancillary sphere to preserve high resolution.
- *Sensitivity with respect to the numerical scheme used for the calculation of droplet trajectories* was analyzed by comparing the results (the values of collision efficiency) obtained using a one-step time-explicit numerical scheme applied in the calculations, with the results obtained using the time consuming Runge-Kutta scheme of the 5-th-order with the automatic choice of time steps. Simulations showed that the simple scheme provided the same values of collision efficiency.
- *Sensitivity to the initial separation distance between droplets.* Supplemental experiments indicate that the utilization of the initial separation distance of ~ 30-40 largest droplet radii, instead of the separation distance of ~10 radii of the largest droplet, results in a few percent change in collision efficiencies. These results indicate that that the HDI zone falls well into elementary volumes. Therefore, calculations were performed with the initial separation distance equal to ~10 radii of the largest droplet.
- *Sensitivity with respect to the size of the ancillary sphere.* The analysis of a great number of simulations showed that utilization of the ancillary sphere with the maximum radius of $3(a_1 + a_2)$ was suitable for actually any combinations of acceleration-shear and droplet radii. Further increase of the ancillary sphere radius did not affect collision efficiency.
- *Verification of the modified superposition method* has been performed in several boundary cases. In the absence of HDI, the method reproduces the values of the swept volume calculated with accuracy better than 0.1% (see Pinsky et al 2006a). For the pure gravity case, the difference between the values of collision efficiency obtained using eqs. (8a-c) and those obtained using the classical method (Pinsky et al 2001) is about 3% and does not exceed 5%. An important evidence of the validity of the calculations is that $E(a_1, a_2) = E(a_2, a_1)$, which means that the algorithm is invariant with respect to the choice of droplets indices a_1 and a_2.
- *Sensitivity to the volume of statistics.* Sensitivity experiments with different volumes of statistical information related to turbulent shear flows indicate that the increase of statistical data set in addition to the set used in the present study ($2.5 \cdot 10^3$ for the calculation of average values and 10^5 for the calculation of PDF) has a negligible effect on the results. Relative errors are within the range 0.4-3%.

We believe, therefore, that the overall error in the calculation of the collision efficiency and the collision kernel does not exceed a few percent.

4. RESULTS

4.1 The magnitudes of the collision efficiencies and collision kernels

Collision efficiencies were calculated for the turbulent conditions typical of clouds. Probability distribution functions of collision efficiency and collision kernels were performed in Pinsky et al (2006b). We present here the dependences of averaged values of the collision efficiencies and kernels on drop size, dissipation rate and Re_λ. **Figure 4** shows the collision efficiencies between 15 μm -(left) and 20 μm -radii (right) collectors with smaller droplets under different dissipation rates and Re_λ. The pure gravity values of the collision efficiencies are shown as well. One can see that strong turbulence increases significantly the collision efficiencies between cloud droplets. Especially significant increase in the collision efficiency takes place for droplets of close size.

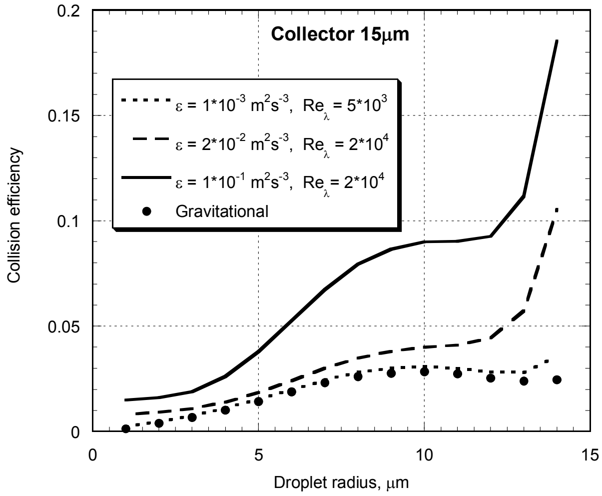

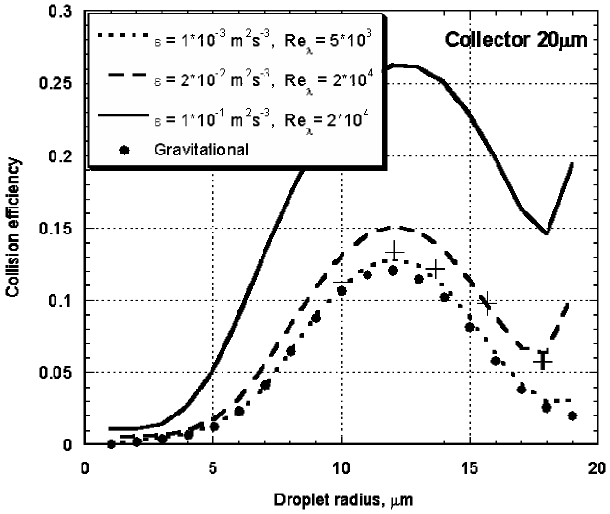

Figure 4. Collision efficiencies between 15-μm (first) and 20-μm radii (second) collectors with smaller droplets under different dissipation rates and Re_λ (after Pinsky et al 2006b). Results obtained by Wang et al (2005) for $\varepsilon = 100 cm^2 s^{-3}$ are marked by crosses on the second panel.

Comparison of the values of collision efficiencies obtained by Pinsky and Khain (2006b) calculated under the conditions relatively to those used by Wang et al (2005a) ($\varepsilon = 100 cm^2 s^{-3}$, drop collector radius 20 μm) indicates a reasonably good agreement in the results.

Figure 5 shows the dependence of the averaged normalized collision kernel for the 10 μm- and 20 μm- radii droplet pair on the dissipation rate ε under different Re_λ.

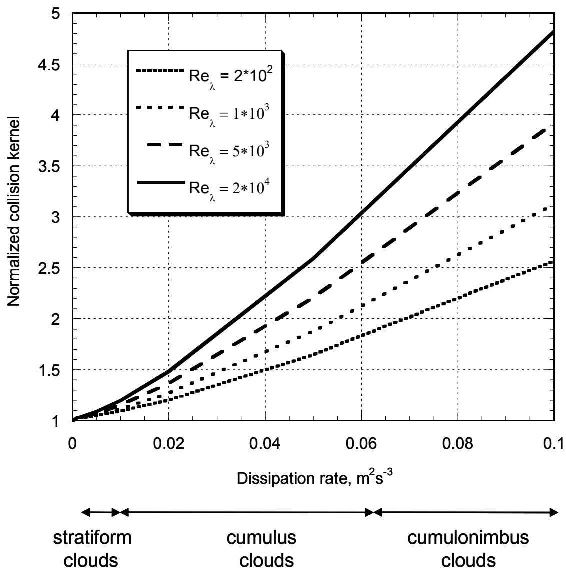

Figure 5. *Dependence of the averaged normalized collision kernel for the 10 μm- and 20 μm- radii droplet pair on the dissipation rate ε under different Re_λ (after Pinsky et al 2006b).*

While the factor of the swept volume increase was found to be 1.6 at very strong turbulence intensity (Pinsky et al 2006a), the collision kernel increases by the factor as large as 4.8. Thus, the effect of turbulence on the HDI appears to be the main mechanism by means of which turbulence increases the rate of cloud droplets collisions. Note that the 10 μm-20 μm-radii droplet pair indicates the minimum turbulent enhancement factor. The increase in the collision kernel of droplet pairs containing droplets of close size or droplets smaller than ~3 μm in radii is much more pronounced. One can see in Fig. 16 that the collision kernel increases both with the increase in ε and Re_λ. Thus, the accounting for the effect of Re_λ is as important as accounting for the effect of the dissipation rate ε.

Figure 6 shows collision kernel enhancement factor for three typical cases: stratiform clouds ($\varepsilon = 0.001\ m^2 s^{-3}$, $\mathrm{Re}_\lambda = 5 \cdot 10^3$) (upper panel), cumulus clouds ($\varepsilon = 0.02\ m^2 s^{-3}$, $\mathrm{Re}_\lambda = 2 \cdot 10^4$) (middle) and cumulonimbus ($\varepsilon = 0.1\ m^2 s^{-3}$, $\mathrm{Re}_\lambda = 2 \cdot 10^4$) (lower panel).

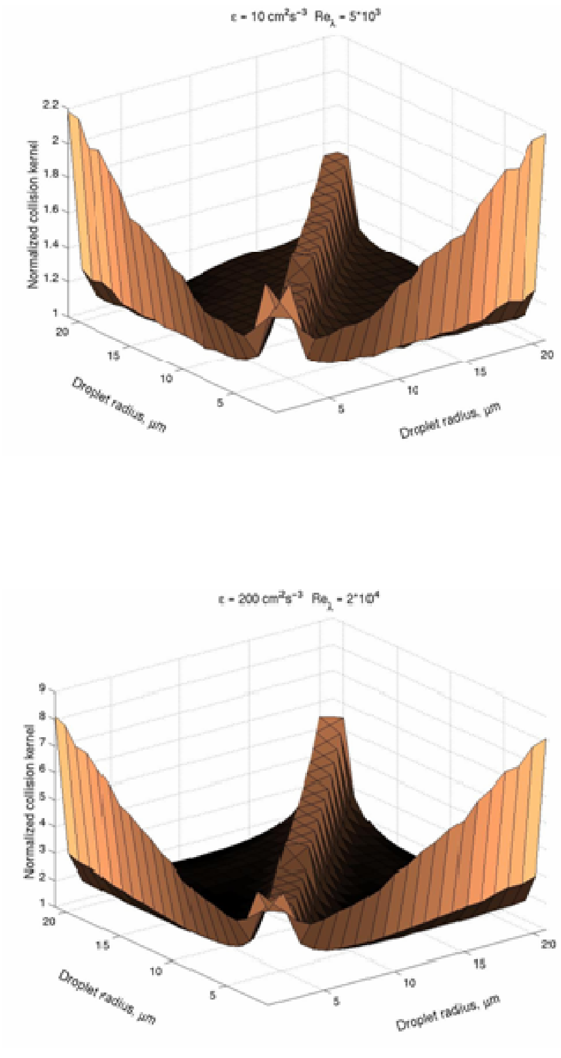

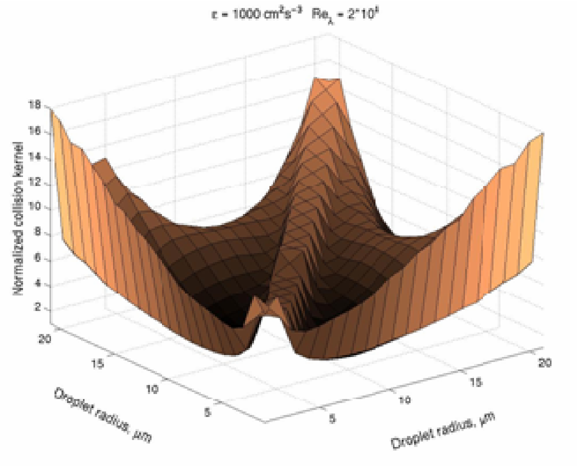

Figure 6. *Collision kernel enhancement factor (as compared to the gravity value) for three typical cases: stratiform clouds* ($\varepsilon = 0.001\ m^2 s^{-3}$, $\mathrm{Re}_\lambda = 5\cdot 10^3$) *(upper panel), cumulus clouds* ($\varepsilon = 0.02\ m^2 s^{-3}$, $\mathrm{Re}_\lambda = 2\cdot 10^4$) *(middle) and cumulonimbus* ($\varepsilon = 0.1\ m^2 s^{-3}$, $\mathrm{Re}_\lambda = 2\cdot 10^4$) *(lower panel).*

The collision kernel enhancement factors are presented in tables 1-3 for corresponding levels of turbulence intensity.

Table 1. Stratocumulus clouds ($\varepsilon = 0.001\ m^2 s^{-3}$, $\mathrm{Re}_\lambda = 5\cdot 10^3$)

	1 μm	2 μm	3 μm	4 μm	5 μm	6 μm	7 μm	8 μm	9 μm	10 μm	11 μm	12 μm	13 μm	14 μm	15 μm	16 μm	17 μm	18 μm	19 μm	20 μm	21 μm
1 μm	1.595	1.719	1.43	1.363	1.366	1.39	1.387	1.404	1.451	1.539	1.559	1.635	1.671	1.722	1.736	1.872	1.951	2.038	2.02	2.169	2.184
2 μm	1.719	1.595	1.471	1.223	1.177	1.151	1.146	1.148	1.13	1.14	1.149	1.149	1.142	1.153	1.149	1.162	1.163	1.21	1.233	1.211	1.254
3 μm	1.43	1.471	1.449	1.427	1.198	1.137	1.12	1.113	1.111	1.107	1.11	1.089	1.109	1.095	1.095	1.083	1.085	1.094	1.081	1.079	1.09
4 μm	1.363	1.223	1.427	1.416	1.404	1.187	1.13	1.12	1.096	1.094	1.101	1.089	1.092	1.101	1.088	1.087	1.072	1.082	1.044	1.047	1.033
5 μm	1.366	1.177	1.198	1.404	1.399	1.394	1.182	1.122	1.114	1.094	1.095	1.086	1.082	1.09	1.077	1.072	1.076	1.069	1.07	1.056	1.045
6 μm	1.39	1.151	1.137	1.187	1.394	1.392	1.39	1.171	1.125	1.107	1.088	1.086	1.079	1.069	1.059	1.044	1.028	1.012	0.998	0.978	0.97
7 μm	1.387	1.146	1.12	1.13	1.182	1.39	1.394	1.398	1.176	1.127	1.103	1.097	1.086	1.071	1.064	1.056	1.05	1.035	1.008	0.961	0.946
8 μm	1.404	1.148	1.113	1.12	1.122	1.171	1.398	1.393	1.388	1.185	1.128	1.098	1.089	1.082	1.082	1.069	1.055	1.019	1.009	0.99	0.968
9 μm	1.451	1.13	1.111	1.096	1.114	1.125	1.176	1.388	1.435	1.483	1.192	1.124	1.091	1.089	1.086	1.072	1.045	1.043	1.025	1.017	0.997
10 μm	1.539	1.14	1.107	1.094	1.094	1.107	1.127	1.185	1.483	1.467	1.452	1.174	1.124	1.096	1.089	1.082	1.071	1.069	1.04	1.025	1.026
11 μm	1.559	1.149	1.11	1.101	1.095	1.088	1.103	1.128	1.192	1.452	1.452	1.453	1.172	1.11	1.091	1.087	1.082	1.08	1.066	1.046	1.04
12 μm	1.635	1.149	1.089	1.089	1.086	1.086	1.097	1.098	1.124	1.174	1.453	1.456	1.46	1.167	1.115	1.09	1.078	1.084	1.08	1.068	1.057
13 μm	1.671	1.142	1.109	1.092	1.082	1.079	1.086	1.089	1.091	1.124	1.172	1.46	1.464	1.468	1.169	1.109	1.093	1.093	1.081	1.081	1.073
14 μm	1.722	1.153	1.095	1.101	1.09	1.069	1.071	1.082	1.089	1.096	1.11	1.167	1.468	1.462	1.455	1.162	1.103	1.087	1.082	1.076	1.08
15 μm	1.736	1.149	1.095	1.088	1.077	1.059	1.064	1.082	1.086	1.089	1.091	1.115	1.169	1.455	1.457	1.459	1.16	1.102	1.09	1.089	1.083
16 μm	1.872	1.162	1.083	1.087	1.072	1.044	1.056	1.069	1.072	1.082	1.087	1.09	1.109	1.162	1.459	1.469	1.479	1.147	1.109	1.09	1.083
17 μm	1.951	1.163	1.085	1.072	1.076	1.028	1.05	1.055	1.045	1.071	1.082	1.078	1.093	1.103	1.16	1.479	1.477	1.476	1.155	1.105	1.088
18 μm	2.038	1.21	1.094	1.082	1.069	1.012	1.035	1.019	1.043	1.069	1.08	1.084	1.093	1.087	1.102	1.147	1.476	1.48	1.484	1.153	1.103
19 μm	2.02	1.233	1.081	1.044	1.07	0.998	1.008	1.009	1.025	1.04	1.066	1.08	1.081	1.082	1.09	1.109	1.155	1.484	1.5	1.516	1.144
20 μm	2.169	1.211	1.079	1.047	1.056	0.978	0.961	0.99	1.017	1.025	1.046	1.068	1.081	1.076	1.089	1.09	1.105	1.153	1.516	1.521	1.525
21 μm	2.184	1.254	1.09	1.033	1.045	0.97	0.946	0.968	0.997	1.026	1.04	1.057	1.073	1.08	1.083	1.083	1.088	1.103	1.144	1.525	1.521

Table 2. Cumulus clouds ($\varepsilon = 0.02\ m^2 s^{-3}, \mathrm{Re}_\lambda = 2 \cdot 10^4$)

	1 µm	2 µm	3 µm	4 µm	5 µm	6 µm	7 µm	8 µm	9 µm	10 µm	11 µm	12 µm	13 µm	14 µm	15 µm	16 µm	17 µm	18 µm	19 µm	20 µm	21 µm
1 µm	4.53	5.075	3.859	3.602	3.64	3.788	3.864	4.018	4.22	4.646	4.809	5.17	5.398	5.729	5.91	6.513	6.853	7.291	7.355	7.961	8.146
2 µm	5.075	4.53	3.985	2.666	2.3	2.137	2.063	2.046	2.028	2.056	2.102	2.155	2.187	2.261	2.311	2.405	2.426	2.578	2.686	2.683	2.844
3 µm	3.859	3.985	3.867	3.748	2.437	2	1.831	1.729	1.664	1.64	1.632	1.6	1.625	1.61	1.624	1.62	1.626	1.667	1.668	1.684	1.725
4 µm	3.602	2.666	3.748	3.698	3.649	2.342	1.903	1.715	1.579	1.522	1.494	1.457	1.449	1.447	1.444	1.458	1.458	1.511	1.518	1.569	1.607
5 µm	3.64	2.3	2.437	3.649	3.633	3.617	2.305	1.844	1.649	1.527	1.468	1.426	1.41	1.427	1.427	1.452	1.502	1.557	1.631	1.693	1.777
6 µm	3.788	2.137	2	2.342	3.617	3.616	3.616	2.279	1.812	1.619	1.492	1.439	1.418	1.429	1.465	1.514	1.575	1.641	1.714	1.763	1.812
7 µm	3.864	2.063	1.831	1.903	2.305	3.616	3.631	3.647	2.281	1.838	1.596	1.498	1.458	1.464	1.514	1.58	1.65	1.699	1.723	1.69	1.64
8 µm	4.018	2.046	1.729	1.715	1.844	2.279	3.647	3.643	3.638	2.39	1.851	1.601	1.509	1.51	1.569	1.632	1.699	1.71	1.658	1.582	1.509
9 µm	4.22	2.028	1.664	1.579	1.649	1.812	2.281	3.638	3.916	4.193	2.488	1.871	1.612	1.562	1.604	1.666	1.711	1.686	1.614	1.528	1.45
10 µm	4.646	2.056	1.64	1.522	1.527	1.619	1.838	2.39	4.193	4.117	4.04	2.417	1.845	1.632	1.619	1.685	1.731	1.686	1.584	1.491	1.427
11 µm	4.809	2.102	1.632	1.494	1.468	1.492	1.596	1.851	2.488	4.04	4.079	4.119	2.428	1.833	1.667	1.696	1.751	1.701	1.594	1.489	1.424
12 µm	5.17	2.155	1.6	1.457	1.426	1.439	1.498	1.601	1.871	2.417	4.119	4.162	4.205	2.425	1.852	1.72	1.756	1.732	1.622	1.511	1.431
13 µm	5.398	2.187	1.625	1.449	1.41	1.418	1.458	1.509	1.612	1.845	2.428	4.205	4.249	4.293	2.443	1.867	1.785	1.789	1.68	1.548	1.455
14 µm	5.729	2.261	1.61	1.447	1.427	1.429	1.464	1.51	1.562	1.632	1.833	2.425	4.293	4.313	4.332	2.45	1.899	1.83	1.758	1.601	1.488
15 µm	5.91	2.311	1.624	1.444	1.427	1.465	1.514	1.569	1.604	1.619	1.667	1.852	2.443	4.332	4.378	4.425	2.466	1.945	1.856	1.704	1.544
16 µm	6.513	2.405	1.62	1.458	1.452	1.514	1.58	1.632	1.666	1.685	1.696	1.72	1.867	2.45	4.425	4.504	4.582	2.48	2.015	1.845	1.639
17 µm	6.853	2.426	1.626	1.458	1.502	1.575	1.65	1.699	1.711	1.731	1.751	1.756	1.785	1.899	2.466	4.582	4.64	4.697	2.545	2.062	1.806
18 µm	7.291	2.578	1.667	1.511	1.557	1.641	1.699	1.71	1.686	1.686	1.701	1.732	1.789	1.83	1.945	2.48	4.697	4.794	4.891	2.612	2.085
19 µm	7.355	2.686	1.668	1.518	1.631	1.714	1.723	1.658	1.614	1.584	1.594	1.622	1.68	1.758	1.856	2.015	2.545	4.891	5.034	5.178	2.677
20 µm	7.961	2.683	1.684	1.569	1.693	1.763	1.69	1.582	1.528	1.491	1.489	1.511	1.548	1.601	1.704	1.845	2.062	2.612	5.178	5.31	5.441
21 µm	8.146	2.844	1.725	1.607	1.777	1.812	1.64	1.509	1.45	1.427	1.424	1.431	1.455	1.488	1.544	1.639	1.806	2.085	2.677	5.441	5.31

Table 3. Cumulonimbus ($\varepsilon = 0.1\ m^2 s^{-3}, \mathrm{Re}_\lambda = 2 \cdot 10^4$)

	1 µm	2 µm	3 µm	4 µm	5 µm	6 µm	7 µm	8 µm	9 µm	10 µm	11 µm	12 µm	13 µm	14 µm	15 µm	16 µm	17 µm	18 µm	19 µm	20 µm	21 µm
1 µm	9.509	10.72	7.719	7.312	7.438	7.774	8.02	8.403	8.937	9.804	10.33	11.12	11.66	12.51	12.91	14.25	15.06	16.07	16.16	17.51	17.96
2 µm	10.72	9.509	8.301	5.267	4.49	4.116	3.975	3.932	3.938	4.02	4.163	4.311	4.412	4.641	4.855	5.155	5.373	5.88	6.354	6.667	7.399
3 µm	7.719	8.301	8.051	7.801	4.771	3.817	3.431	3.236	3.17	3.225	3.374	3.516	3.845	4.15	4.605	5.085	5.704	6.524	7.364	8.358	9.568
4 µm	7.312	5.267	7.801	7.691	7.581	4.578	3.627	3.276	3.139	3.251	3.515	3.847	4.382	5.014	5.732	6.621	7.537	8.811	9.893	11.35	12.74
5 µm	7.438	4.49	4.771	7.581	7.54	7.498	4.526	3.591	3.369	3.46	3.824	4.338	5.016	5.874	6.718	7.681	8.765	9.816	10.94	11.95	13.02
6 µm	7.774	4.116	3.817	4.578	7.498	7.49	7.481	4.519	3.725	3.723	4.052	4.683	5.451	6.331	7.252	8.129	8.936	9.614	10.13	10.34	10.37
7 µm	8.02	3.975	3.431	3.627	4.526	7.481	7.52	7.56	4.63	4.096	4.268	4.894	5.715	6.581	7.475	8.184	8.664	8.771	8.554	7.921	7.238
8 µm	8.403	3.932	3.236	3.276	3.591	4.519	7.56	7.545	7.529	5.057	4.579	4.991	5.805	6.727	7.581	8.078	8.234	7.829	7.059	6.219	5.503
9 µm	8.937	3.938	3.17	3.139	3.369	3.725	4.63	7.529	8.157	8.785	5.539	5.222	5.826	6.775	7.607	8.003	7.823	7.087	6.169	5.33	4.669
10 µm	9.804	4.02	3.225	3.251	3.46	3.723	4.096	5.057	8.785	8.638	8.492	5.716	5.752	6.556	7.433	7.899	7.654	6.733	5.66	4.826	4.247
11 µm	10.33	4.163	3.374	3.515	3.824	4.052	4.268	4.579	5.539	8.492	8.615	8.738	6.173	6.367	7.245	7.896	7.738	6.696	5.534	4.63	4.047
12 µm	11.12	4.311	3.516	3.847	4.338	4.683	4.894	4.991	5.222	5.716	8.738	8.891	9.043	6.656	7.082	7.808	7.929	6.964	5.654	4.646	3.977
13 µm	11.66	4.412	3.845	4.382	5.016	5.451	5.715	5.805	5.826	5.752	6.173	9.043	9.223	9.404	7.275	7.676	8.198	7.596	6.084	4.838	4.046
14 µm	12.51	4.641	4.15	5.014	5.874	6.331	6.581	6.727	6.775	6.556	6.367	6.656	9.404	9.544	9.684	7.871	8.24	8.233	6.845	5.246	4.238
15 µm	12.91	4.855	4.605	5.732	6.718	7.252	7.475	7.581	7.607	7.433	7.245	7.082	7.275	9.684	9.919	10.15	8.533	8.723	7.98	6.078	4.63
16 µm	14.25	5.155	5.085	6.621	7.681	8.129	8.184	8.078	8.003	7.899	7.896	7.808	7.676	7.871	10.15	10.48	10.81	9.152	9.134	7.438	5.375
17 µm	15.06	5.373	5.704	7.537	8.765	8.936	8.664	8.234	7.823	7.654	7.738	7.929	8.198	8.24	8.533	10.81	11.12	11.44	9.96	9.243	6.777
18 µm	16.07	5.88	6.524	8.811	9.816	9.614	8.771	7.829	7.087	6.733	6.696	6.964	7.596	8.233	8.723	9.152	11.44	11.9	12.36	10.69	9.092
19 µm	16.16	6.354	7.364	9.893	10.94	10.13	8.554	7.059	6.169	5.66	5.534	5.654	6.084	6.845	7.98	9.134	9.96	12.36	12.99	13.62	11.33
20 µm	17.51	6.667	8.358	11.35	11.95	10.34	7.921	6.219	5.33	4.826	4.63	4.646	4.838	5.246	6.078	7.438	9.243	10.69	13.62	14.25	14.88
21 µm	17.96	7.399	9.568	12.74	13.02	10.37	7.238	5.503	4.669	4.247	4.047	3.977	4.046	4.238	4.63	5.375	6.777	9.092	11.33	14.88	14.25

One can see that collision enhancement factor is quite significant, especially for drops of close sizes as well as for droplets of very different sizes.

Collision enhancement factors were calculated for 500 mb level as well. The enhancement factor at 500 mb level is larger than that for 1000 mb level by factors 1.5-2 that agrees with the results obtained by Pinsky et al (2001). The factor increases because the increase in the relative sedimentation velocity caused by the decrease of air density with height.
Note that enhancement factors presented in Figure 6 and tables 1-3 were calculated with no effect of droplet clustering.

4.2 Parameterization of droplet clustering effect

To parameterize effects of droplet clustering in a turbulent flow we used an empirical dependence of clustering intensity on the St number, presented by Pinsky and Khain (2003). The dependence has been obtained as a result of statistical analysis of a long series of drop arrival times measured in situ in ~60 cumulus clouds. The parameterization formula is as follows:

$$\frac{\left\langle N'^2 \right\rangle^{1/2}}{\left\langle N \right\rangle} = f(St) = 0.577 \cdot St^{0.317}, \qquad (10)$$

where $\left\langle N \right\rangle$ is the cloud averaged droplet concentration, $\left\langle N'^2 \right\rangle^{1/2}$ is the r.m.s. of the concentration fluctuations.
Under assumption of strong spatial correlation of concentration fluctuations of cloud droplets of different size, we introduced a “correction” factor of the collision kernel between droplets characterized by the Stokes numbers St_1 and St_2 as follows:

$$G(St_1, St_2) = \frac{\left\langle N_1 N_2 \right\rangle}{\left\langle N_1 \right\rangle \left\langle N_2 \right\rangle} = 1 + f(St_1) f(St_2) = \qquad (11)$$
$$= 1 + 0.333 \cdot (St_1 St_2)^{0.317}$$

Function $G(St_1, St_2)$ depends on both droplet sizes and on the intensity of turbulence (on the dissipation rate).

4.3 Examples of droplet spectrum evolution

To illustrate effects of turbulence on DSD development and raindrop formation we integrated the stochastic collision equation (12)

$$\frac{df}{dt} = \frac{1}{2} \int_0^{m/2} \left\langle f(m') f(m - m', m') \right\rangle K(m - m', m') dm' - \qquad (12)$$
$$- \int_0^{\infty} \left\langle f(m) f(m') \right\rangle K(m, m') dm'$$

for the period of 30 min. In (12) f is the DSD function. Two droplet spectra typical of intermediate (droplet concentration N=500 cm^{-3}, CWC=1.8 gm^{-3}) and more continental clouds (N=800 cm^{-3}, CWC=2.3 gm^{-3}) were chosen. The initial DSD are centered at radii of ~ 9 μm. Calculations were performed both for pure gravity case, as well as for turbulent conditions. The calculations under turbulent conditions were performed both with and without effects of droplet clustering taken into account. In simulations without the clustering effect $\langle f(m_1)f(m_2)\rangle$ was calculated as $\langle f(m_1)\rangle\langle f(m_2)\rangle$ in accordance with the common practice in cloud modeling. To take the clustering effect into account the expression $\langle f(m_1)f(m_2)\rangle$ has been multiplied by factor $G(St_1, St_2)$ determined in (11). In all turbulent simulations collision kernel $K(m_1, m_2)$ has been multiplied by the enhancement factors presented in Tables 1-3.

Note that turbulence effects were taken into account only for cloud droplets with radii below 21 μm. No changes for drops of larger size were made. Thus, the result possibly underestimates the turbulent effect. At the same time, it allows us to evaluate effects of turbulence on formation of large cloud droplets and small raindrops which trigger precipitation formation.

Results of calculations are presented in Figure 7, showing DSD obtained toward t=30 min. in simulations mentioned above.

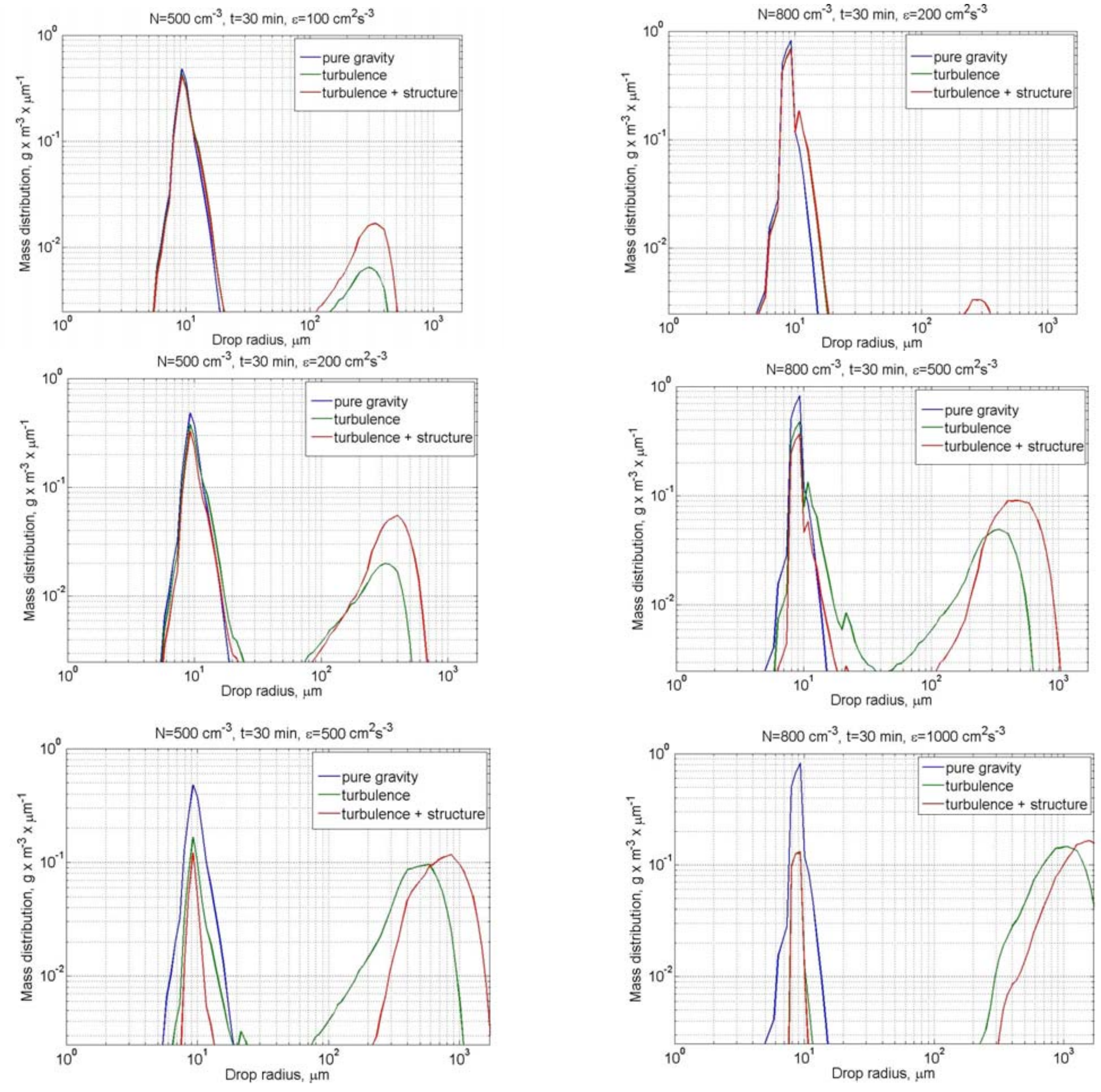
N=500 cm^{-3}, t=30 min, ε=100 cm^{2}s^{-3}

N=800 cm^{-3}, t=30 min, ε=200 cm^{2}s^{-3}

N=500 cm^{-3}, t=30 min, ε=200 cm^{2}s^{-3}

N=800 cm^{-3}, t=30 min, ε=500 cm^{2}s^{-3}

N=500 cm^{-3}, t=30 min, ε=500 cm^{2}s^{-3}

N=800 cm^{-3}, t=30 min, ε=1000 cm^{2}s^{-3}

Figure 7. DSDs obtained by solving the stochastic collision equation during t=30 min. DSD obtained toward t=30 min in case of pure gravity case are marked by green. Three values of the dissipation rate were used: $\varepsilon = 0.01\ m^2 s^{-3}, 0.02\ m^2 s^{-3}, 0.05\ m^2 s^{-3}\ and\ 0.1\ m^2 s^{-3}$. DSD obtained when collision kernel enhancement is determined only by HDI and transport effect (Tables 1-3) are marked by green. DSDs obtained when the enhancement factor by clustering effect is taken into account is marked by red.

One can see that at high droplet concentration and low turbulent intensity the effect of turbulence is not significant (at least during the time period of 30 min). Turbulence of larger intensity significantly accelerates collisions, indicating the formation of raindrops, while no raindrops were formed in pure gravity case.

5. CONCLUSIONS

The collision efficiencies and collision kernels were calculated for conditions typical of real cloud of different type for 1-21 micron- radii droplets. Detailed tables of collision kernel enhancement are presented.

A parameterization of the effect of droplet concentration fluctuation is proposed. The method is based on statistical analysis of in situ data in 60 clouds.

Effect of turbulence is illustrated by calculation of droplet size distribution evolution using a stochastic collision equation. A significant acceleration of rain formation in a turbulent flow was demonstrated for droplet spectra typical of intermediate and continental clouds. It is shown that increase in the collision rate between cloud droplets may serve as a triggering mechanism for raindrop formation, at least for not extremely maritime clouds.

The tables of the collision kernel enhancement factors are available upon request.

Acknowledgements

The study was supported by the Israel Science Foundation (grant 173/03) and the European Project ANTISTORM. The authors are grateful to Prof. N. Kleeorin for valuable discussions and to Professor M. Tegmark who provided us with codes for sphere pixelization.

REFERENCES

Almeida, F. C., 1979: The collisional problem of cloud droplets moving in a turbulent environment-part II: Turbulent collision efficiencies. *J. Atmos. Sci.,* **36**, 1564-1576.

Belin F, Maurer J, Tabeling P. and Willaime H. 1997: Velocity gradient distributions in fully developed turbulence: An experimental study, *Phys. Fluids,* **9**, 3843-3850

Franklin, C.N., P.A. Vaillancourt, M.K. Yau and P. Bartello, 2004: Cloud droplet collision rates in evolving turbulent flows, *14-th International conference on Clouds and Precipitation,* Bologna, Italy, 19-23 July 2004, 520-523.

Hill, R. J, 2002: Scaling of acceleration in locally isotropic turbulence, *J. Fluid Mech*., **452**, 361-370.

Khain, A., M. Ovtchinnicov, M. Pinsky, A. Pokrovsky and H. Krugliak, 2000: Notes on the state-of-the-art numerical modeling of cloud microphysics. *Atmos. Res*. , **55**, 159-224.

Koziol, A. S., and H. G. Leighton, 1996: The effect of turbulence on the collision rates of small cloud drops, *J. Atmos. Sci.* , **53**, 1910-1920

La Porta A., G.A. Voth, A. M. Crawford, J. Alexander and E. Bodenschatz 2001: Fluid particle accelerations in fully developed turbulence, *Nature*, **409**, 1017-1019

Langmuir, I, 1948: The production of rain by a chain reaction in cumulus clouds at temperature above freezing. *J. Meteorol,* **5**, 175–192

Lin, C.L. and S.C Lee, 1975: Collision efficiency of water drops in the atmosphere*. J. Atmos. Sci.,* **32**, 1412–1418

Pinsky, M. B., and A. P. Khain, 2003: Fine structure of cloud droplet concentration as seen from the Fast-FSSP measurements. Part 2: Results of in-situ observations*, J. Appl. Meteor*., **42**, 65-73.

Pinsky M.B., and A.P. Khain, 2004: Collisions of small drops in a turbulent flow. Part 2. Effects of flow accelerations*, J. Atmos. Sci.,* **61**, 1926-1939.

Pinsky, M., A. P. Khain, and M. Shapiro, 1999a: Collisions of small drops in a turbulent flow. Pt.1: Collision efficiency: problem formulation and preliminary results*, J. Atmos. Sci*., **56**, 2585-2600

Pinsky, M., A.P. Khain, and M. Shapiro, 2000: Stochastic effects on cloud droplet hydrodynamic interaction in a turbulent flow, *Atmos. Res.,* **53**, 131-169

Pinsky, M., A. P. Khain, and M. Shapiro 2001: Collision efficiency of drops in a wide range of Reynolds numbers: Effects of pressure on spectrum evolution*. J. Atmos. Sci*. **58**, 742-764

Pinsky M., Shapiro M., Khain A. and Wirzberger H., 2004: A statistical model of strains in homogeneous and isotropic turbulence, Physica D, **191**, 297-313

Pinsky M. B., A. P. Khain , B. Grits and M. Shapiro, 2006a: “Collisions of cloud droplets in a turbulent flow. Part 3. Relative droplet fluxes and swept volumes”, J. Atmos. Sci (in press).

Pinsky M., Khain A. and Shapiro M, 2006b: Collisions of cloud droplets in a turbulent flow. Part 4. Droplet hydrodynamic interaction*. J. Atmos. Sci.* (Submitted).

Pruppacher, H. R., and J. D. Klett, 1997: *Microphysics of clouds and precipitation.* 2-nd edition, Oxford Press, 1997, 963p.

Shaw R.A., 2003: Particle-turbulence interactions in atmospheric clouds, *Annu. Rev. Fluid Mech*., **35**, 183-227.

Shafrir, U. and T. Gal-Chen, 1971: A numerical study of collision efficiencies and coalescence parameters for droplet pairs with radii up to 300 microns*. J. Atmos. Sci.,* **28**, 741–751

Schlamp, R.J. Grover S.N., Pruppacher H.R. and Hamielec, A.E., 1976: A electric charges and vertical external fields on the collision efficiency of cloud drops. *J. Atmos. Sci.,* **33**, 1747-1755.

Tegmark M., 1996: An icosahedron-based method for pixelizing the celestial sphere, *Astophys. J.,* **470,** L81-L84.

Wang, L-P, O. Ayala, S.E. Kasprzak, and W.W. Grabowski, 2005a: Theoretical formulation of collision rate and collision efficiency of hydrodynamically interacting cloud droplets in turbulent atmosphere. *J. Atmos. Sci*. **62**, 2433-2450.

Wang, L-P., O. Ayala, and W.W. Grabowski, 2005: On improved formulations of the superposition method, *J. Atmos. Sci*. ,**62**, 1255-1266.

Vaillancourt P.A., and Yau M. K., 2000: Review of particle-turbulence interactions and consequences for Cloud Physics, *Bull. Am. Met. Soc.,* **81**, 285-298

Vohl, O., S.K. Mitra, S.C. Wurzler and H.R. Pruppacher, 1999: A wind tunnel study on the effects of turbulence on the growth of cloud drops by collision and coalescence*, J. Atmos. Sci*., **56**, 4088-4099.